Research in Astron. Astrophys. **20xx** Vol. **9** No. **XX**, 000–000
http://www.raa-journal.org *http://www.iop.org/journals/raa*

***R**esearch in*
***A**stronomy and*
***A**strophysics*

arXiv:1404.3016v1 [astro-ph.SR] 11 Apr 2014

Investigation of Star Formation toward the Sharpless 155 H II region

Ya Fang Huang[1], Jin Zeng Li[1], Travis A. Rector[2] and Zhou Fan[1]

[1] National Astronomical Observatories, Chinese Academy of Sciences, Beijing 100012, China; *huangyf@nao.cas.cn*

[2] University of Alaska Anchorage, 3211 Providence Drive, Anchorage, AK 99508 USA

Received 2013 November 21; accepted 2014 April 10

Abstract We present a comprehensive study of star formation toward the H II region S155. Star-formation activities therein were investigated based on multi-wavelength data from optical to the far-infrared. The surface density distribution of selected 2MASS sources toward S155 indicates the existence of a compact cluster, which is spatially consistent with the position of the exciting source of the H II region, HD 217086. A sample of more than 200 excessive emission sources in the infrared were selected based on their 2MASS color indices. The spatial distribution of the sample sources reveals the existence of three young sub-clusters in this region, among which, sub-cluster A is spatially coincident with the bright rim of the H II region. In addition, photometric data from the WISE survey were used to identify and classify young stellar objects (YSOs). To further explore the evolutionary stages of the candidate YSOs, we fit the spectral energy distribution (SEDs) of 44 sources, which led to the identification of 14 Class I, 27 Class II, and 3 Class III YSOs. The spatial distribution of the classified YSOs at different evolutionary stages presents a spatio-temporal gradient, which is consistent with a scenario of sequential star formation. On the other hand, Herschel PACS observations toward the interface between S155 and the ambient molecular cloud disclose an arc-shaped dust layer, the origin of which could be attributed to the UV dissipation from the early type stars e.g. HD 217061 in S155. Four dusty cores were revealed by the Herschel data, which hints for new generations of star formation.

Key words: ISM: H II regions — stars: formation — stars: pre-main sequence — infrared: stars

1 INTRODUCTION

Cepheus (Cep) OB3 is a very young association at a distance of about 800 pc from the Sun (Moreno-Corral et al., 1993). It covers a region from $22^h46^m00^s$ to $23^h10^m00^s$ in right ascension and from $+61^\circ$ to $+64^\circ$ in declination. It is mainly composed of two subgroups: the older, Cep OB3a, the largest projected dimension of which is about 17 pc, and the younger, Cep OB3b, more compact and closer to Cep molecular cloud (Pozzo et al., 2003). Cep OB3 association has always been considered to be a very good example of large-region sequential star formation according with the model of Elmegreen & Lada (1977), where supernova remnants and stellar winds of an older stellar cluster compress the ambient clouds and trigger the formation of a second generation of stars (Sargent, 1979).

The interface between Cep OB3b and the Cep molecular cloud is clearly delineated by the optically bright H II region Sharpless 155 (S155, see Figure 1), where neutral material is ionized and

heated by the radiation of the O7 star HD 217086 and the illumination star, HD 217061 (Lynds & Oneil, 1986). Both of them belong to the youngest generation of the Cep OB3b association (Panagia & Thum, 1981). The photodissociation region (PDR) at S155 is favorably oriented to reveal the progression of star formation. Near-infrared studies (Moreno-Corral et al., 1993; Testi et al., 1995),CO (Minchin et al., 1992),far-infrared, and radio continuum (Felli et al., 1978; Testi et al., 1995) have revealed a few young stellar objects (YSOs) embedded in the Cep cloud behind the PDR. Sources with high extinction have been detected on the edge of the Cep molecular cloud. They maybe represent a third generation of star formation triggered by the expansion of the H II region. This scenario of triggered star formation has been recently strengthened by Getman et al. (2006, 2009) with the Chandra X-ray surveys and Spitzer archived data.

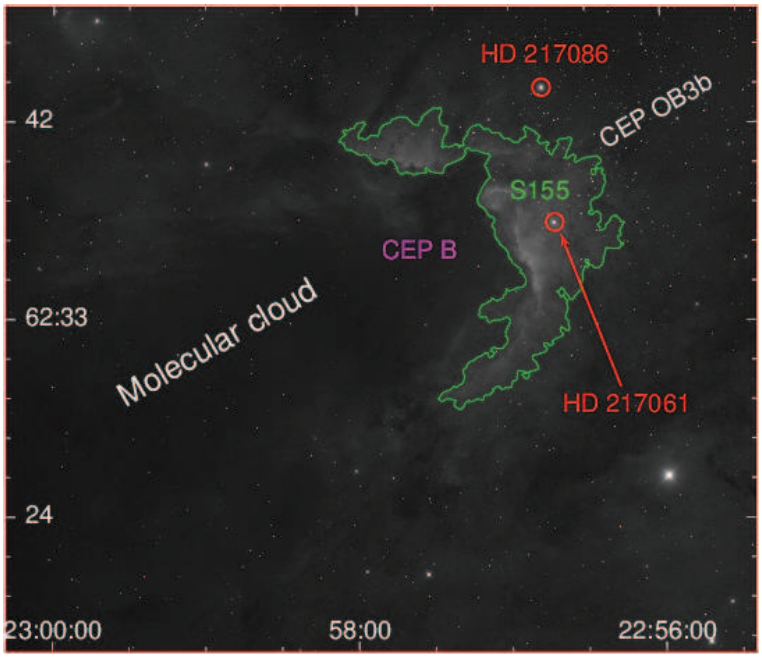

Fig. 1 Hα narrow band image covering $30' \times 30'$ of the S155 and its nearby region. Cep B, the hottest component of the Cep molecular cloud, is located in the center of the field. Cep OB3b, the younger subgroup of Cep OB3 association, lies to the northwest. The interface between the molecular cloud and Cep OB3b is delineated by the H II region, S155. And the exiting stars HD 217086 and the illumination star HD 217061 are labeled. North is up; east is to the left.

In this paper, we present and discuss the scenario of sequential and triggered star formation in S155 and its nearby region based on 2MASS, WISE and the Herschel PACS data. Surface density distribution of the 2MASS PSC sources presents the existence of compact clusters of pre-main sequence stars (PMS). The WISE photometric data help to remove contaminants and fit spectral energy distributions (SEDs), and the Herschel PACS data present cold dusty cores which hints for new generations of star formation.

We present in Section 2 optical imaging of S155 as well as details of the retrieval of archival 2MASS and WISE data. In Section 3, we discuss the spatial distribution of the sub-clusters toward S155. SED classification of the sample sources follows in Section 4. The results achieved are discussed in Section 5 and summarized in Section 6.

2 DATA ACQUISITION AND ANALYSIS

2.1 Narrowband Imaging

S155 was observed with the MOSAIC camera on the Mayall 4-meter telescope at Kitt Peak National Observatory. MOSAIC is an optical camera. It consists of eight 2048×4096 CCD detectors arranged to form a 8192×8192 array with 35-50 pixel wide gaps between the CCDs. With a scale of $0\farcs26$ pixel^{-1}, the field of view is about $36' \times 36'$. To fill in the bad columns and gaps, all observations are completed in a five-exposure dither pattern with offsets of 100 pixels.

Observations toward S155 were obtained on 9 September 2009 with the "Nearly-Mould" I (MOSAIC filter k1005), Hα (k1009) and [SII] (ha16, H-alpha+16nm, k1013) filters, whose central wavelengths/FWHMs are 6574.74/80.62, 6730.72/81.1, and 8204.53/1914.59 Å, respectively. Five exposures of 300 sec were obtained in Hα and [SII]. And five 180 sec exposures were obtained in I.

2.2 2MASS JHKs photometry

Infrared (IR) sources in the field of S155 were found using archival data from the 2MASS PSC. To ensure the reliability of the extracted sources, we employed the following strict requirements in the sample selection, which are revised based on the criteria presented by Li & Smith (2005a): (1) $[JHK_S]_cmsig \leq 0.1$ (corrected JHK_S band photometric uncertainty less than or equal to 0.1 mag) (2) $K_S_snr > 15$ (K_S band "scan" signal-to-noise ratio greater than 15).

2.3 WISE photometry

The Wide-field Infrared Survey Explorer (WISE) is a NASA medium-class explorer mission, launched on 2009 December 14 (Wright et al., 2010; Jarrett et al., 2011). WISE mapped the entire sky simultaneously in four bands centered at 3.4, 4.6, 12, and 22 μm (W1, W2, W3, and W4) with 5σ point-source sensitivities of approximately 0.08, 0.1, 1, and 6 mJy (Koenig et al., 2012).

In this paper, the sample of excessive emission sources selected based on the 2MASS data is cross-identified with the WISE All-Sky Source Catalog using the simple positional correlation method with a $3''$ search radius (Koenig et al., 2012). The following sample selection criterion was employed to guarantee the reliability of the WISE data in use and to allow a rigorous analysis. Only sources with certain detection in all four bands (W1 W2 W3$_{sigmpro} \leq 0.1$ and W4$_{sigmpro} \leq 0.5$) were considered.

3 CLUSTERING OF STAR FORMATION IN S155

Figure 1 shows the Hα image of a $30' \times 30'$ region surrounding S155. The bright portion delineated with a green line is the H II region which is the interface between the Cep B molecular cloud and the association Cep OB3b. In this section, we will explore the 2MASS sources in the field shown in Figure 1.

3.1 Color-color diagram

In the target region, 2MASS database contains more than ten thousands photometric detections. We narrowed down the catalogue to 4481 sources using the select criteria mentioned in Section 2.

2MASS JHK_S color-color (C-C) diagram has been widely used to select sources with IR excessive emissions. Figure 2 shows the C-C diagram for S155. All the 2MASS sources that match our criteria are put into the JHK_S C-C diagram and denoted as dots. We defined 217 objects as YSO candidates for they are located below the right line of the normal star reddening band and $H - K_S > 0.3$ in the C-C diagram. Those sources are selected for they possess intrinsic color excesses likely originating from emission of circumstellar dust, commensurate with their embedded nature. The color distinction helps to eliminate foreground field stars and narrowed the YSO candidates sample.

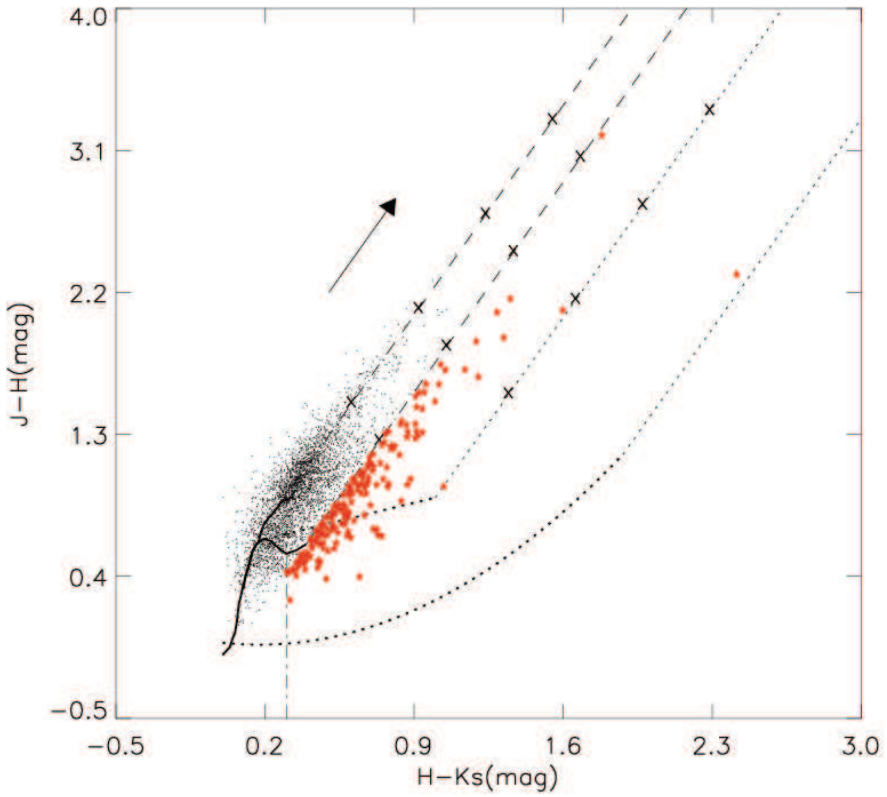

Fig. 2 $(J-H)$ vs. $(H-K_S)$ C-C diagram of S155. The sample sources are denoted as dots. Selected IR excessive emission sources are labeled in red. Black solid lines represent the loci of the MS dwarfs and giant stars (Bessell & Brett, 1988). Two paralleled dashed lines define the reddening band for normal stars. The arrow shows a reddening vector of $A_v = 5$ mag (Rieke & Lebofsky, 1985). The left dotted line indicates the locus of dereddened T Tauri star (Meyer et al., 1997) and its reddening band boundary. The right dotted line indicates the locus of dereddened HAeBe (Lada & Adams, 1992) and its reddening direction. Crosses were over plotted with an interval corresponding to 5 mag of visual extinction.

3.2 Surface density distribution

Shown in Figure 3 (a) is the surface density map of all the validly detected 2MASS sources in the targeted region. Irregular distribution of sources is prominently visualized. There is a cavity in the center and a enhancement in the top-right corner. This prominently dense region is labeled with a large red circle and having the exciting star HD 217086 enclosed. There are about 12 sources in 0.75×0.75 arcmin^2 at the densest region, which coincides with the location of Cep OB3b. However, the structure of the H II region is not revealed in this panel.

In Figure 3 (b), the spatial distribution of the YSO candidates, there are three densest regions revealed. Combined with the trichromatic image from the Mayall 4-meter telescope of KPNO presented in panel (c), the three subclusters all surround Cep OB3b region, likely be triggered by the stellar winds from those OB stars. Compared to cluster B and C, subcluster A corresponds to the bright rim marked in panel (c), and is more compact and brighter, which may contains younger star formation activity.

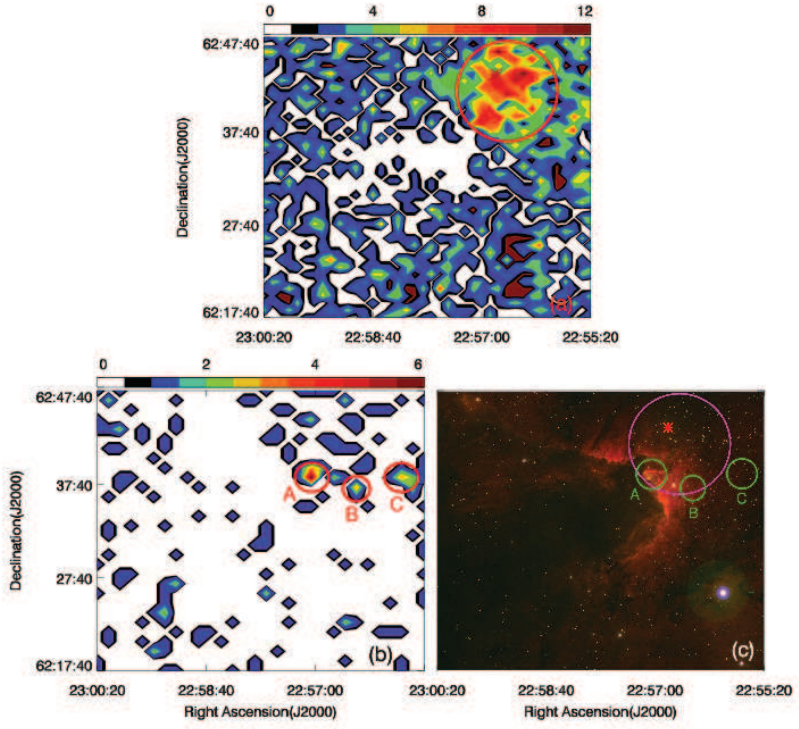

Fig. 3 (a) Surface density distribution of the 2MASS sources toward S155. The densest region at the top right corner marked with a large red circle is consistent with the position of Cep OB3b, and the asterisk indicates HD 217086 (R.A.= $22^h56^m47^s.19$, decl.= $+62°43'37''.64$(J2000)). The color bar indicates the number of sources in every 0.75×0.75 arcmin^2. (b) Spatial distribution of the 217 2MASS excessive emission sources. Red circles mark the three densest regions of YSO candidates, which harbor active star formation. (c) Trichromatic image of S155 generated from I (blue), [SII] (green), and Hα (red) band image observed with the Mayall 4-meter telescope of KPNO. Red asterisk indicates the main exciting source HD 217086.

4 IDENTIFICATION AND CLASSIFICATION OF EXCESS EMISSION SOURCES IN S155

4.1 Selection of YSOs based on WISE photometry

Koenig et al. (2012) have developed a scheme to identify YSOs based on WISE colors and magnitudes. With this scheme, contaminants can be removed and YSO candidates can be roughly classified. Contaminants arises from non-YSO sources, including star-forming galaxies, broad-line active galactic nuclei (AGNs), unresolved knots of shock emission from outflows colliding with cold cloud material, planetary nebulae, and asymptotic giant branch (AGB) stars (Koenig et al., 2012). And YSOs can be classified into the canonical categories of Class I, Class II, with supplemental categories of "deeply embedded sources"(added to the Class I tallies) and "transition disks" (objects with optically thick excess emission at long wavelengths and little to no excess at short wavelengths, Strom et al., 1989). After cross-identified with WISE data, 55 sources remain in the YSO candidates sample. Based on the scheme, 11 contaminants were removed and 44 were classified as YSOs.

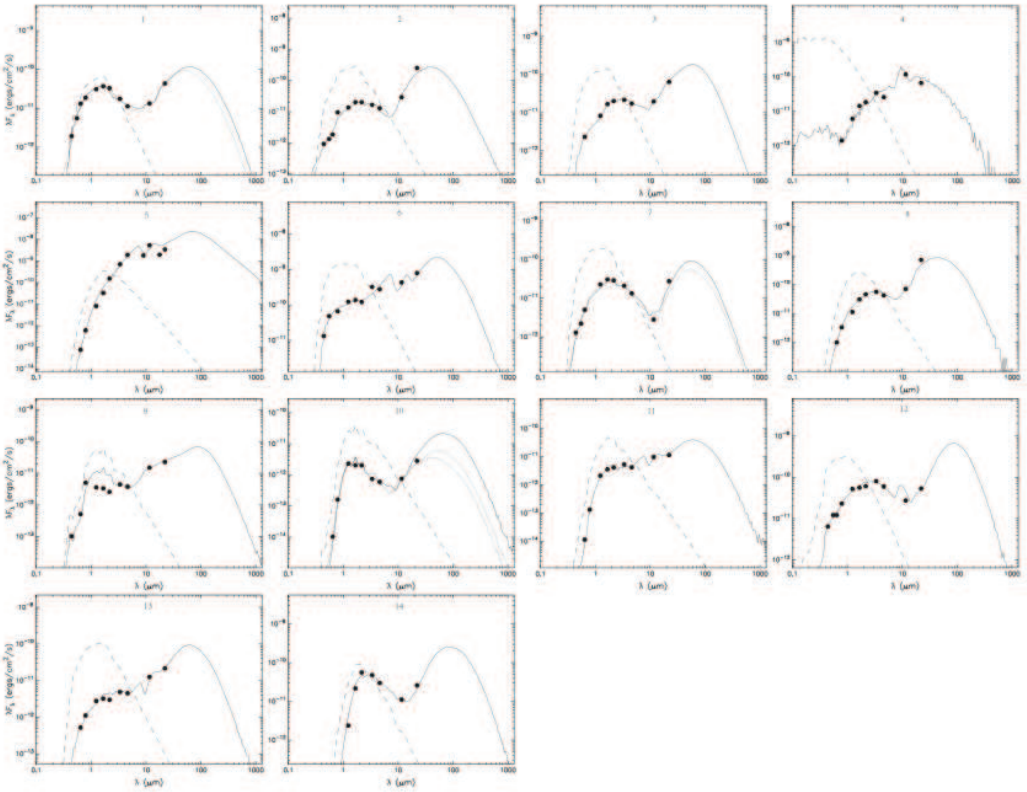

Fig. 4 Results of the SED fitting for the sample sources. The black dots show the measured fluxes currently available. The solid black curve represents the best model fitting of the data points with the smallest χ^2. The gray curves indicate the other potential model fitting results with χ^2/N-$\chi^2_{best}/N<$ 3. The dashed curve gives the photosphere that is used as input for the radiative transfer code.

4.2 Classification based on SED fitting

To more accurately determine their evolutionary status, the SEDs of the 44 YSOs are fitted. Robitaille et al. (2006) developed a grid of 200,000 YSO models to fit the SED from optical to millimeter wavelengths. Those models span a wide range of evolutionary stages for different stellar masses. They also provide a linear regression tool, by which we can select all model SEDs that fit the observed SED better than a specified χ^2 (Robitaille et al., 2006).

Lada (1987) developed a widely used classification scheme for YSOs, based on the "four staged" star formation scenario proposed by Shu et al. (1987). With an evolutionary sequence from early type to late type, YSOs were classified into Class I to III, primarily based on their SEDs. Robitaille et al. (2006) presented a classification scheme refers to the actual evolutionary stage of the object based on physical properties. However, in view of the differences between observable and physical properties, we primarily refer the ages fitted by the tool and the slope of its near/mid-IR SED. Class I sources refer to objects whose $Age \approx 10^5$ yr and $Slope_{near/mid-IR} > 0$, Class II sources refer to $Age \approx 10^6$ yr and $Slope_{near/mid-IR} \leq 0$, and Class III is for objects whose SED is similar to a black-body spectrum.

Multi-wavelength online archived data are used for SED fitting. In addition to WISE and 2MASS PSC data, we used: 1) IRAC and MIPS photometry at 3.6, 4.5, 5.8, 8 and 24m for a few of sources; 2) the far-IR IRAS Point Sources photometry at 12, 25, 60 and 100μm; 3) the mid-IR A (8.28 μm), C (12.13 μm), D (14.65 μm) provided by the MSX6C IR PSC, and S9W (9 μm), L18W (18 μm) provided

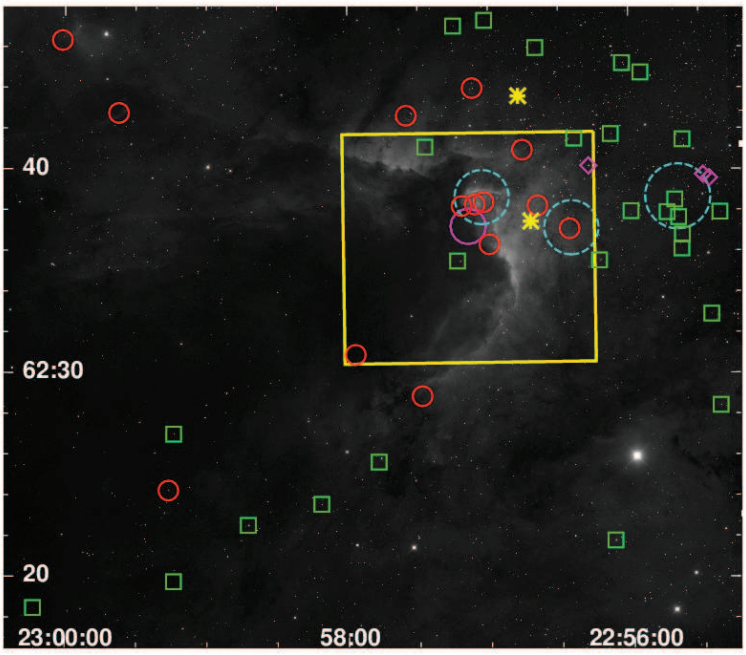

Fig. 5 Distribution of YSOs classified based on SEDs. CLASS I, II, and III sources are indicated with red circles, green boxes, and magenta diamonds, respectively. The yellow asterisks indicate HD 217086 (upper) and HD 217061. Cyan dashed circles present the three subclusters marked in Figure 3. Magenta circle is the location of the dense core in Cep B molecular. The Herschel PACS image region is outlined in yellow.

by the AKARI IRC PSC; 4) BVR photometry from the Naval Observatory Merged Astrometric Dataset (NOMAD). As a result, SEDs are fitted with a photometric catalogue over a large wavelength range. The PMS nature and evolutionary status of all the YSO candidates have been confirmed and corrected by results of the SED fittings (Table 1). Figure 4 illustrates the SED of the CLASS I sources of the sample.

5 DISCUSSION

5.1 Sequential and triggered star formation around S155

In this work, we provide new additional evidence to support a scenario of sequential and triggered star formation in S155. Figure 5 presents the Hα image of S155, on which the sample sources classified based on SEDs are overlaid with different symbols. The spatial distribution of the classified sources reveals a dramatic spatiotemporal gradient: younger stars (Class I sources) are clustered in the H II region S155, while older stars (Class II and Class III sources) are dispersed in the other side of the primary ionizing star HD 217086. Of the considered locations of three subclusters in Figure 3, region A is indeed younger and more compact than the other two. Furthermore, most of the identified CLASS I and CLASS II sources are located along the edge of the molecular cloud. All these characters are consistent with a triggered nature of star and cluster formation in this region.

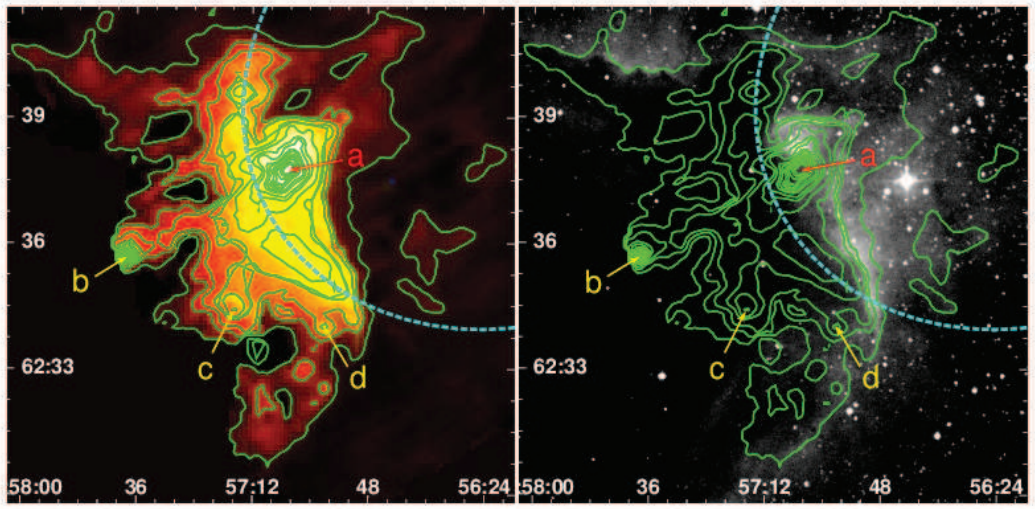

Fig. 6 Left: Color composite image of S155 and its nearby region in Herschel PACS 160 μm (red), 70 μm (green) and WISE W3 12 μm (blue). Right: DSS 2 red band image of target region. Green contours in both two images are generated from the Herschel PACS image in 160 μm band.

5.2 New generation star formation

To further investigate the interstellar materials within the molecular cloud, Herschel PACS (Poglitsch et al., 2010) images of a region outlined in Figure 5 were employed. The left panel of Figure 6 presents the composite image of this target region, which was compiled with the PACS 160 μm (red), 70 μm (green) and WISE W3 (blue) imaging data. It is evident that the dark edge of the molecular cloud in the DSS-2 red band image (left panel in Figure 6) is bright in emission in the far-IR. This indicates the existence of large amount cold dust and star formation activity. The overlaid contours generated based on the Herschel PACS image indicate the presence of four far-IR cores. Among those bright cores, core "a" is spatially consistent with the location of dense core in Cep B molecular cloud. Behind this dense core, an arc-shaped bright layer surround it and face to HD 217061. Its origin could be attributed to the compression from the feedback of HD 217061 to the molecular cloud. Based on distribution of them and other three cores, we infer that new generations of star formation is going on in the edge of molecular cloud, the morphology of the bright part is both effected by the illumination star HD 217061 and dense core.

Based on these evidences, the scenario of the sequential and triggered star formation in the whole S155/Cep OB3b region is clear. Due to the influence of Cep OB3a, the first generation of the OB stars were born in Cep OB 3b, which contains HD 217086 and HD 217061. Then the wind originating from these stars compressed the surrounding cloud to trigger the second generation of stars (region A, B, and C marked in Figure 3). On the east of Cep OB3b, a bright arc of nebulosity was produced for the existence of Cep molecular cloud, and defined the interface between the S155 H II region and the Cep B molecular cloud (Pozzo et al., 2003). As the surface of the cloud is being eroded, primarily by the illumination star HD 217061, the cloud edge moves eastward across the observer's field of view, with the third generation stars emerging from the obscuring molecular cloud (bright cores presented in Figure 6).

6 SUMMARY

We present a comprehensive study of sequential and triggered star formation toward the H II region S155. The sample of excessive emission sources are selected based on archived 2MASS data, which

is then cross-identification with the WISE PSC. SED fittings are employed to further classify the IR sources. In the target region, we identify 14 Class I, 27 Class II and 3 Class III sources, 20 of which are newly discovered.

The spatial distribution of the IR excessive emission sources selected based on their 2MASS colors reveals the existence of three sub-clusters in this region, which may have a triggered origin due to their spatial distribution as respect to the massive cluster Cep OB3b. Compared with the other two subclusters, region A is spatially associated with the brightest part of S155 and harbors the most Class I sources, which supports the conclusion that A might be younger than the other two regions. This is supported by the observation it is located on the interface between S155 and Cep B molecular cloud. Based on the spatial distribution of the classified YSOs, all Class I sources are found to located within S155, while the Class II sources are distributed on the outer edges of the HII region, which suggests a scenario of sequential and/or triggered star formation in this region. Furthermore, four far-IR cores and a bright arc were discovered by the Herschel PACS data, which provide evidence for new generations of star formation.

Acknowledgements We appreciate very much the helpful comments and suggestions from the referee. This work employed data from 2MASS, WISE, Herschel and other astronomical databases. Our investigation is supported by funding from the National Natural Science Foundation of China (Grant Nos. 11073027 and 11003021), Beijing Natural Science Foundation (1144015) and the Department of International Cooperation of the Ministry of Science and Technology of China (Grant No. 2010DFA02710). The Mayall 4-meter telescope at Kitt Peak National Observatory is a facility of the National Optical Astronomy Observatory, which is operated by the Association of Universities for Research in Astronomy, Inc. (AURA) under cooperative agreement with the National Science Foundation.

Table 1. Photometry and classification of YSO sample sources.

ID	R.A.(J2000.0)	Dec.(J2000.0)	J (mag)	H (mag)	Ks (mag)	W1 (mag)	W2 (mag)	W3 (mag)	W4 (mag)	M[d] ($M_\odot$)	Class SEDs
(1)	(2)	(3)	(4)	(5)	(6)	(7)	(8)	(9)	(10)	(11)	12
1[a]	22 56 25.74	62 37 07.0	12.739 ± 0.021	11.754 ± 0.022	11.122 ± 0.02	10.493 ± 0.026	9.993 ± 0.023	6.973 ± 0.019	3.539 ± 0.037	0.72	I
2[b]	22 56 39.30	62 38 15.0	13.632 ± 0.019	12.397 ± 0.022	11.648 ± 0.02	10.556 ± 0.024	9.833 ± 0.02	6.115 ± 0.019	1.623 ± 0.027	1.16	I
3[a]	22 56 45.65	62 40 59.1	14.166 ± 0.03	12.599 ± 0.021	11.651 ± 0.018	10.265 ± 0.027	9.514 ± 0.022	6.552 ± 0.039	3.117 ± 0.064	0.73	I
4[a]	22 56 59.85	62 36 20.8	14.512 ± 0.033	12.769 ± 0.023	11.744 ± 0.018	9.765 ± 0.029	9.084 ± 0.021	4.605 ± 0.017	3.077 ± 0.161	0.8	I
5[a]	22 57 02.20	62 38 25.1	14.182 ± 0.052	11.868 ± 0.039	9.453 ± 0.019	6.48 ± 0.024	4.426 ± 0.022	0.473 ± 0.022	-1.2 ± 0.007	3.01	I
6[a]	22 57 05.94	62 38 18.0	11.244 ± 0.02	10.316 ± 0.021	9.713 ± 0.016	7.329 ± 0.01	6.514 ± 0.009	3.201 ± 0.075	0.385 ± 0.023	2.48	I
7[a]	22 57 06.87	62 44 00.8	13.071 ± 0.022	11.949 ± 0.021	11.256 ± 0.018	10.3 ± 0.023	9.806 ± 0.02	8.661 ± 0.077	4.034 ± 0.06	0.73	I
8[a,c]	22 57 11.54	62 38 13.6	13.827 ± 0.026	11.937 ± 0.02	10.745 ± 0.016	9.22 ± 0.033	8.537 ± 0.032	5.146 ± 0.095	0.497 ± 0.025	2.08	I
9	22 57 28.67	62 28 54.1	15.08 ± 0.052	14.348 ± 0.051	13.875 ± 0.063	11.98 ± 0.024	11.177 ± 0.022	6.837 ± 0.018	4.25 ± 0.026		I
10	22 57 35.03	62 42 39.9	15.559 ± 0.067	14.903 ± 0.076	14.154 ± 0.066	13.929 ± 0.033	13.174 ± 0.034	10.089 ± 0.06	6.502 ± 0.081		I
11	22 57 56.81	62 30 56.2	15.637 ± 0.069	14.27 ± 0.053	13.364 ± 0.042	11.779 ± 0.029	11.043 ± 0.035	7.302 ± 0.086	4.967 ± 0.066		I
12	22 59 16.17	62 24 15.4	12.171 ± 0.021	11.293 ± 0.031	10.453 ± 0.021	8.836 ± 0.023	8.177 ± 0.02	6.184 ± 0.034	3.313 ± 0.038		I
13	23 00 01.24	62 46 19.9	15.351 ± 0.061	14.388 ± 0.071	13.718 ± 0.055	11.884 ± 0.03	10.977 ± 0.031	7.042 ± 0.018	4.299 ± 0.031		I
14	22 59 37.21	62 42 46.3	15.523 ± 0.067	12.327 ± 0.032	10.545 ± 0.02	9.4 ± 0.022	8.932 ± 0.019	7.167 ± 0.029	4.097 ± 0.026		I
15	22 55 22.49	62 28 25.1	14.19 ± 0.026	13.072 ± 0.025	12.331 ± 0.023	11.064 ± 0.022	10.494 ± 0.021	8.215 ± 0.057	6.307 ± 0.08		II
16	22 55 38.15	62 36 06.3	15.055 ± 0.037	13.763 ± 0.037	12.845 ± 0.023	11.636 ± 0.023	10.986 ± 0.02	9.105 ± 0.032	7.077 ± 0.094		II
17[a]	22 55 55.00	62 44 45.8	15.558 ± 0.072	13.994 ± 0.039	13.071 ± 0.028	11.685 ± 0.024	10.947 ± 0.021	8.574 ± 0.028	6.336 ± 0.063	0.25	II
18[a]	22 56 23.57	62 41 32.6	13.377 ± 0.025	12.286 ± 0.028	11.606 ± 0.023	10.433 ± 0.026	9.916 ± 0.02	7.622 ± 0.022	4.803 ± 0.035	0.53	II
19	22 55 21.78	62 37 53.5	12.693 ± 0.019	11.381 ± 0.021	10.442 ± 0.018	9.427 ± 0.023	8.575 ± 0.019	6.197 ± 0.016	4.266 ± 0.024		II
20	22 55 25.89	62 32 53.8	12.546 ± 0.019	11.599 ± 0.02	10.962 ± 0.014	10.174 ± 0.023	9.626 ± 0.021	7.224 ± 0.018	5.072 ± 0.03		II
21[a]	22 55 37.45	62 41 28.0	12.567 ± 0.027	11.249 ± 0.023	10.468 ± 0.018	9.129 ± 0.023	8.399 ± 0.018	6.546 ± 0.012	4.828 ± 0.028	1.81	II
22	22 55 37.88	62 36 47.5	15.666 ± 0.066	14.362 ± 0.053	13.597 ± 0.039	12.599 ± 0.025	11.958 ± 0.023	10.416 ± 0.068	7.77 ± 0.185		II
23[b]	22 55 39.40	62 37 39.0	14.077 ± 0.03	12.97 ± 0.032	12.286 ± 0.022	11.293 ± 0.023	10.676 ± 0.021	9.058 ± 0.03	6.696 ± 0.065	0.61	II
24[b]	22 55 40.87	62 38 30.7	15.758 ± 0.072	14.584 ± 0.067	13.876 ± 0.052	12.829 ± 0.026	12.143 ± 0.025	10.351 ± 0.057	7.986 ± 0.232	0.24	II
25[b]	22 55 44.17	62 37 53.8	15.208 ± 0.05	14.239 ± 0.052	13.463 ± 0.034	12.424 ± 0.025	11.737 ± 0.023	10.348 ± 0.06	7.507 ± 0.135	0.25	II
26[b]	22 55 59.56	62 37 57.2	14.818 ± 0.039	13.946 ± 0.039	13.34 ± 0.039	12.581 ± 0.026	12.051 ± 0.024	10.195 ± 0.057	6.517 ± 0.07	0.28	II
27[a]	22 56 02.81	62 45 13.7	13.338 ± 0.024	12.282 ± 0.023	11.631 ± 0.02	10.705 ± 0.023	10.09 ± 0.02	8.066 ± 0.026	6.097 ± 0.066	0.51	II
28	22 56 07.67	62 21 48.2	10.44 ± 0.024	9.47 ± 0.024	8.431 ± 0.017	6.931 ± 0.034	6.09 ± 0.024	2.989 ± 0.014	1.149 ± 0.013		II
29[a]	22 56 07.98	62 41 45.1	13.069 ± 0.019	11.86 ± 0.019	11.064 ± 0.018	10.107 ± 0.023	9.351 ± 0.02	7.274 ± 0.02	5.313 ± 0.036	0.93	II
30[a]	22 56 13.18	62 35 33.1	11.805 ± 0.019	10.781 ± 0.019	10.122 ± 0.017	8.994 ± 0.022	8.47 ± 0.02	6.576 ± 0.017	3.987 ± 0.028	1.88	II
31	...	...	...	...	...	...	...	...	...	...	...

*Table 1 is published in its entirety in the electronic edition. A portion is shown here for guidance regarding its form and content.

[a]Sources detected by Getman et al. (2006).

[b]Sources detected by Getman et al. (2009).

[c]Sources detected by Moreno-Corral et al. (1993).

[d]From the results of Getman et al. (2006) and Getman et al. (2009).

References

Bessell, M. S., & Brett, J. M. 1988, PASP, 100, 1134
Beuther, H., Kramer, C., Deiss, B., & Stutzki, J. 2000, A&A, 362, 1109
Blaauw, A. 1964, ARA&A, 2, 213
Elmegreen, B. G., & Lada, C. J. 1977, ApJ, 214, 725
Evans, N. J., II, Slovak, M. H., Becklin, E. E., et al. 1981, ApJ, 244, 115
Fabian, A. C., & Stewart, G. C. 1983, MNRAS, 202, 697
Felli, M., Tofani, G., Harten, R. H., & Panagia, N. 1978, A&A, 69, 199
Getman, K. V., Feigelson, E. D., Townsley, L., et al. 2006, ApJS, 163, 306
Getman, K. V., Feigelson, E. D., Luhman, K. L., et al. 2009, ApJ, 699, 1454
Heyer, M. H., Carpenter, J., & Ladd, E. F. 1993, Bulletin of the American Astronomical Society, 25, 1333
Hunt, L. K., Lisi, F., Felli, M., & Tofani, G. 1993, Mem. Soc. Astron. Italiana, 64, 739
Jarrett, T. H., Cohen, M., Masci, F., et al. 2011, ApJ, 735, 112
Jordi, C., Trullols, E., & Galadi-Enriquez, D. 1996, A&A, 312, 499
Kenyon, S. J., & Hartmann, L. 1995, ApJS, 101, 117
Koenig, X. P., Leisawitz, D. T., Benford, D. J., et al. 2012, ApJ, 744, 130
Kun, M., Kiss, Z. T., & Balog, Z. 2008, Handbook of Star Forming Regions, Volume I, 136
Lada, C. J. 1987, in Proc. Symp. on Star FormingRegions, Vol. 115, ed. M. Peimbert & J.Jugaku (Dordredcht: Reidel), 1
Lada, C. J., & Adams, F. C. 1992, ApJ, 393, 278
Li, J. Z., & Smith, M. D. 2005, A&A, 431, 925
Lynds, B. T., & Oneil, E. J., Jr. 1986, PASP, 98, 1294
Meyer, M. R., Calvet, N., & Hillenbrand, L. A. 1997, AJ, 114, 288
Minchin, N. R., Ward-Thompson, D., & White, G. J. 1992, A&A, 265, 733
Moreno-Corral, M. A., Chavarria, K. C., de Lara, E., & Wagner, S. 1993, A&A, 273, 619
Naylor, T., & Fabian, A. C. 1999, MNRAS, 302, 714
Panagia, N., & Thum, C. 1981, A&A, 98, 295
Poglitsch, A., Waelkens, C., Geis, N., et al. 2010, A&A, 518, L2
Pozzo, M., Naylor, T., Jeffries, R. D., & Drew, J. E. 2003, MNRAS, 341, 805
Sargent, A. I. 1977, ApJ, 218, 736
Sargent, A. I. 1979, ApJ, 233, 163
Sharpless, S. 1959, ApJS, 4, 257
Shu, F. H., Adams, F. C., & Lizano, S. 1987, araa, 25, 23
Stapelfeldt, K., Sahai, R., Werner, M., & Trauger, J. 1997, Planets Beyond the Solar System and the Next Generation of Space Missions, 119, 131
Strom, K. M., Strom, S. E., Edwards, S., Cabrit, S., & Skrutskie, M. F. 1989, AJ, 97, 1451
Testi, L., Olmi, L., Hunt, L., et al. 1995, A&A, 303, 881
Wright, E. L., Eisenhardt, P. R. M., Mainzer, A. K., et al. 2010, AJ, 140, 1868
Rieke, G. H., & Lebofsky, M. J. 1985, ApJ, 288, 618
Robitaille, T. P., Whitney, B. A., Indebetouw, R., Wood, K., & Denzmore, P. 2006, ApJS, 167, 256